Controlled Hydroxy-Fluorination Reaction of Anatase to Promote Mg^{2+} Mobility in Rechargeable Magnesium Batteries

Jiwei Ma, Toshinari Koketsu, Benjamin. J. Morgan, Christophe Legein, Monique Body, Peter Strasser and Damien Dambournet*

Electronic Supplementary Information

Table of content

1. Synthesis

Anatase featuring different compositions/vacancy concentrations have been prepared following a previously reported method.[1,2] Briefly, 1.2 mL aqueous hydrofluoric acid solution was added to the mixture of 24.8 mL isopropanol and 4 mL titanium isopropoxide in the Teflon liner cup within a stainless-steel autoclave. After sealing the autoclave, the mixed solution was heated inside an oven at 90 °C and 130 °C for 12 h, respectively. After cooling down to room temperature, the obtained white precipitates were washed with ethanol and centrifuged, then dried at 100 °C under air for 10 h. The recovered samples were further outgassed at 150 °C overnight under primary vacuum prior to physico-chemical and electrochemical characterizations. X-ray diffraction patterns (Figure S1) confirmed the phase purity. To determine the chemical composition, we assessed the vacancy content by structural analysis of total scattering data, evaluated the fluorine content using solid-state ^{19}F NMR and the OH content was deduced according to the general chemical formula $Ti_{1-x-y}\square_{x+y}O_{2-4(x+y)}F_{4x}(OH)_{4y}$.[3]

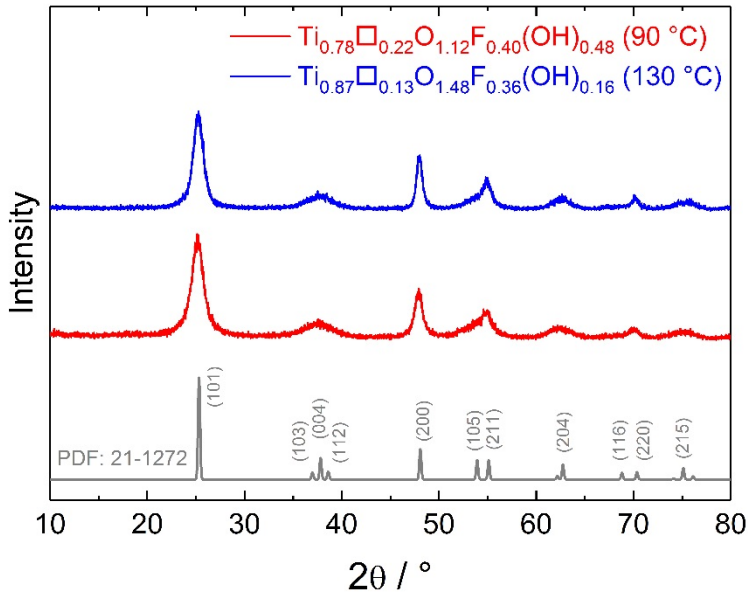

Figure S1. X-ray diffraction patterns of the samples prepared at 90 and 130 °C.

Chemical magnesiation was performed according to the previously reported procedure.[4] Briefly, ethylmagnesium bromide solution (3.0 M in diethyl ether, Sigma-Aldrich) was added drop-by-drop to a solution containing diethyl ether and the solid host $Ti_{0.78}\square_{0.22}O_{1.12}F_{0.4}(OH)_{0.48}$. The mixture was stirred for 48 hours at room temperature. The obtained powder was collected by filtration, washed with anhydrous diethyl ether solvent, and dried under vacuum. All subsequent operations were carried out in an argon-filled glove box.

2. Electrochemistry

Swagelok-type three-electrode cell was used for the electrochemical characterization. The working electrode was composed of 80 wt% active material, 10 wt% conductive carbon (SuperP, Timcal), and 10 wt% polyvinylidene difluoride (PVDF, Aldrich). The suspension of those chemicals in *N*-methyl-2-pyrrolidone (NMP, Sigma-Aldrich) was hand milled using a mortar, and then drop coated on a Mo foil (99.95%, Alfa Aeser) at the geometrical active mass density of 2 mg cm^{-2}. Mg metal plate (99.9%, Good fellow) was used as the reference electrode and the counter electrode. 0.2 mol L^{-1} 2PhMgCl – $AlCl_3$ / THF was prepared by dropping 0.5 mol L^{-1} $AlCl_3$ / THF (Sigma-Aldrich) into 2 mol L^{-1} PhMgCl / THF (Sigma-Aldrich) under agitation for 12 hours, and it was used as the electrolyte, and borosilicate glass-fiber filter paper (Whatmann grade GF/A) was used as the separator. The measurements were carried out at 25 °C. Galvanostatic discharge-charge measurements were performed at different current densities in the potential range of 0.05-2.3 V vs. Mg^{2+}/Mg, and the specific capacities were calculated based on the mass of the active material on the electrode.

3. Galvanostatic Intermittent Titration Technique

Galvanostatic intermittent titration (GITT)[5–7] experiments were performed for the first discharge **(Figure S2)**. In these experiments, a current density of 10 mA g^{-1} was applied for 1h followed by a 10h relaxation period from the open circuit voltage to 0.05 V. Diffusion coefficient was estimated according to the following equation:

$$D_{\mathrm{GITT}}(x) = \frac{4}{\pi}\left(\frac{IV_{\mathrm{M}}}{zFS}\right)^2\left(\frac{dE(x)/dx}{dE(t)/dt^{1/2}}\right)^2 \qquad (t \ll L/D_{\mathrm{GITT}}) \qquad (1)$$

Here, F is Faraday's constant, z is charge number of Mg (z = 2), S is the surface area of electrode, I is the current, V_{M} is the molar volume of the host lattice, and L is characteristic length of electrode materials.

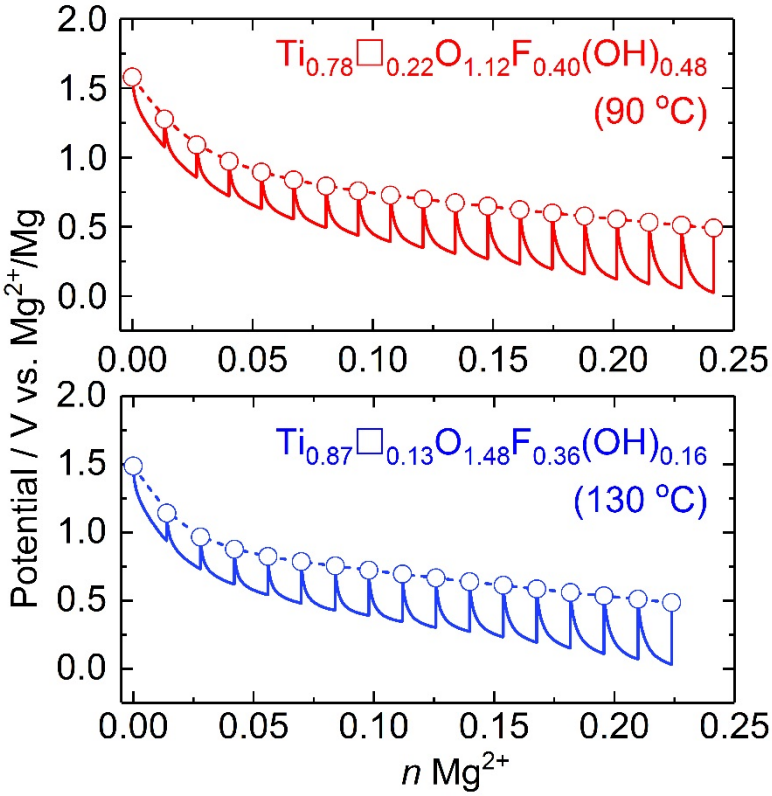

Figure S2. Voltage-composition profiles obtained using the galvanostatic intermittent titration technique (GITT) recorded during the first discharge for $Ti_{0.78}\square_{0.22}O_{1.12}F_{0.40}(OH)_{0.48}$ (90 °C) and $Ti_{0.87}\square_{0.13}O_{1.48}F_{0.36}(OH)_{0.16}$ (130 °C) compounds.

4. ^{19}F solid state NMR

4.1 Experimental details

Experimental details about the ^{19}F solid-state magic angle spinning (MAS) NMR spectrum of $Ti_{0.78}\square_{0.22}O_{1.12}F_{0.40}(OH)_{0.48}$ have been reported previously.[1] ^{19}F solid-state MAS NMR experiments on chemically magnesiated samples were performed on a Bruker Avance III spectrometer operating at 7.0 T (^{19}F Larmor frequency of 282.2 MHz), using a 2.5 mm CP-MAS probe head. Samples were kept in a dry glove box under nitrogen atmosphere and the rotors were filled inside the glove box to avoid any hydration of the samples. As the samples are paramagnetic, all spectra were recorded at high spinning frequencies (≥ 30 kHz) to enhance the sensitivity and resolution.[8] ^{19}F MAS NMR spectra were acquired using a Hahn echo sequence with an interpulse delay equal to one rotor period and a one pulse sequence. The 90° pulse length was set to 1.75 µs and the recycle delay was set to 20 s. Depending on the samples and sequences, between 128 and 512 scans were accumulated. ^{19}F MAS NMR spectra are referenced to $CFCl_3$ and they were fitted with the DMFit software.[9]

5.2 ^{19}F solid state NMR spectra of $Ti_{0.78}\square_{0.22}O_{1.12}F_{0.40}(OH)_{0.48}$ and chemically magnesiated samples

The ^{19}F NMR spectra (**Figure S3**) of the pristine ($Ti_{0.78}\square_{0.22}O_{1.12}F_{0.40}(OH)_{0.48}$) and magnesiated samples ($Mg_{0.07}Ti^{IV}_{0.68}Ti^{III}_{0.14}\square_{0.15}O_{1.12}F_{0.40}(OH)_{0.48}$ and $Mg_{0.13}Ti^{IV}_{0.52}Ti^{III}_{0.26}\square_{0.09}O_{1.12}F_{0.40}(OH)_{0.48}$) reveal the disappearance of the line characteristic of $Ti^{IV}\square_2$-F species (from or even before 0.07 Mg^{2+} per formula unit) and a strong intensity decrease for the resonance assigned to $Ti^{IV}_2\square$-F species. This evidences a filling of the vacancies by Mg^{2+}, preferentially and firstly in di-vacancy systems (becoming single-vacancies). Based on the ^{19}F isotropic chemical shift (δ_{iso}) values of the environments $Ti^{IV}\square_2$-F, $Ti^{IV}_2\square$-F and Ti^{IV}_3-F in $Ti_{0.78}\square_{0.22}O_{1.12}F_{0.40}(OH)_{0.48}$,[1] Mg_3-F in MgF_2 (δ_{iso} = -197.3 ppm).[10] and Ti^{III}_2-F in TiF_3 (δ_{iso} = -144.8 ppm)[4] and on the decrease of the δ_{iso} value of fluoride anions when the number of surrounding cations increases, the insertion of Mg^{2+} ion in a titanium vacancy and the reduction of a Ti^{4+} ion into a Ti^{3+} ion are both expected to induce a decrease of the δ_{iso} value of the neighboring fluorine. And actually, when the content of Mg^{2+} increases, the relative intensities of the NMR resonances of higher (smaller) chemical shift decrease (increase). Concomitantly, a broad resonance appears at ~ -180 ppm. This isotropic chemical shift value is between those for Ti^{III}_2-F environment in TiF_3 and Mg_3-F environment in MgF_2. These observations are consistent with the formation of new fluorine environments with different numbers of surrounding Mg^{2+}, Ti^{IV}, Ti^{III} species and vacancies.

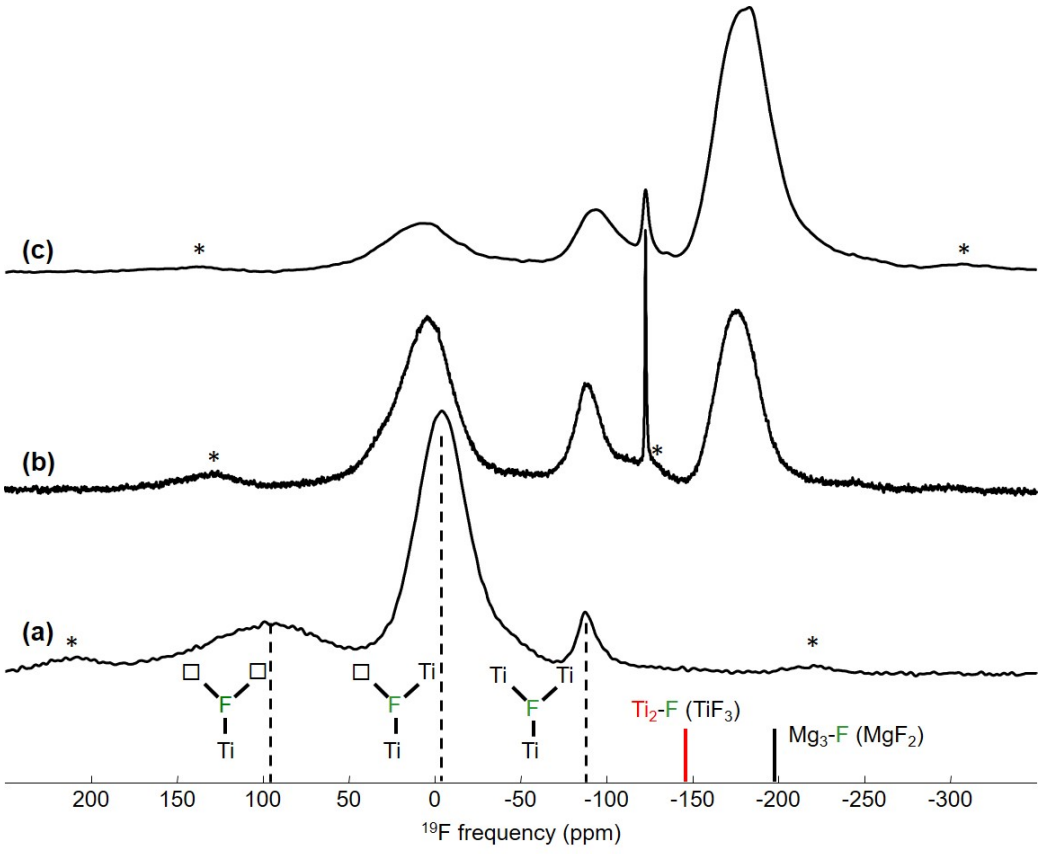

Figure S3. Experimental ^{19}F solid-state MAS NMR spectra of **(a)** $Ti_{0.78}\square_{0.22}O_{1.12}F_{0.40}(OH)_{0.48}$ (60 kHz) and chemically magnesiated samples **(b)** $Mg_{0.07}Ti_{0.78}\square_{0.15}O_{1.12}F_{0.40}(OH)_{0.48}$ (34 kHz) **(c)** $Mg_{0.13}Ti_{0.78}\square_{0.09}O_{1.12}F_{0.40}(OH)_{0.48}$ (34 kHz). The asterisks indicate the main spinning sidebands. The dashed lines indicate the ^{19}F δ_{iso} values of Ti^{IV}_3-F, $Ti^{IV}_2\square$-F, and $Ti^{IV}\square_2$-F (Ti^{IV} are in black) environments in $Ti_{0.78}\square_{0.22}O_{1.12}F_{0.40}(OH)_{0.48}$.[1] Solid lines indicate the ^{19}F δ_{iso} values of Ti^{III}_2-F environment in TiF_3 and Mg_3-F environment in MgF_2.[4,10] Tentative assignment of the NMR resonances to the various species which are supposed to occur in the chemically magnesiated samples and fits of the spectra **(a)** and **(c)** have been reported previously.[4] The fit of the spectrum (b) is presented in **Figure S4**.

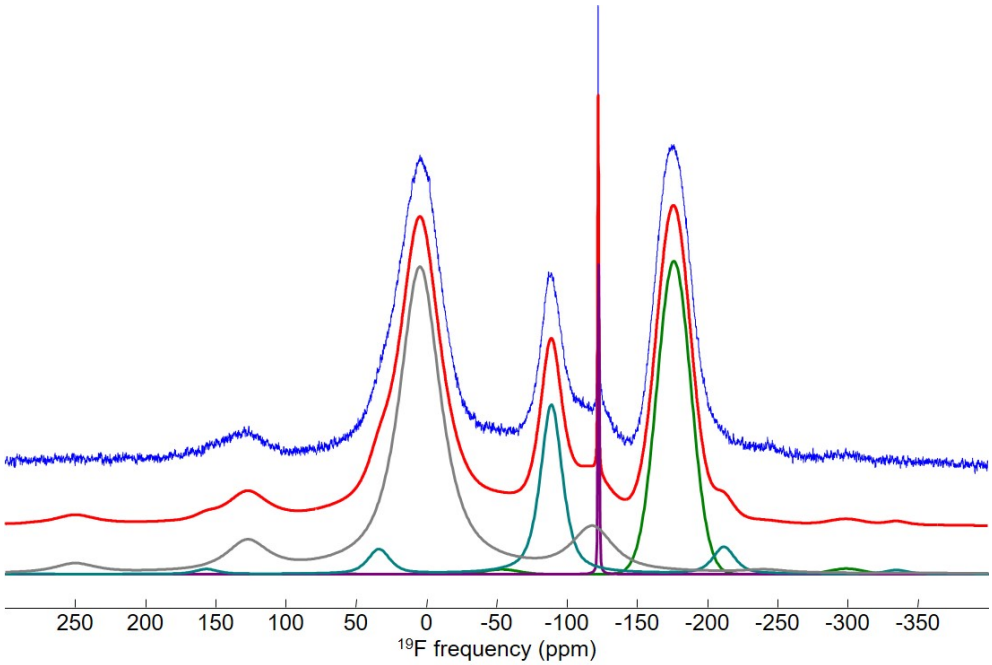

Figure S4. Experimental and fitted ^{19}F MAS (34 kHz) NMR spectra of $Mg_{0.07}Ti_{0.78}\square_{0.15}O_{1.12}F_{0.40}(OH)_{0.48}$. The individual resonances used for the fit are shown below (see **Table S2**).

Table S1. Isotropic chemical shifts δ_{iso} (ppm), line widths LW (ppm), and relative intensities I (%) of the NMR lines obtained from the reconstruction of the ^{19}F solid state MAS (34 kHz) NMR spectrum of $Mg_{0.07}Ti_{0.78}\square_{0.15}O_{1.12}F_{0.40}(OH)_{0.48}$ and tentative assignment of these NMR lines.

δ_{iso} (±0.5)	LW (±0.5)	I (±0.5)	Assignment
-176.2	28.2	27.7	$Ti^{IV}Ti^{III}_2$-F, Ti^{III}_2Mg-F, $Ti^{III}Mg_2$-F, $Ti^{IV}_2Ti^{III}$-F, $Ti^{III}_2\square$-F, $Ti^{IV}Ti^{III}$Mg-F, $Ti^{IV}Mg_2$-F
-122.5	1.0	1.4	Adsorbed F^-

-88.9	18.5	16.3	Ti^{IV}_3-F, $Ti^{IV}Ti^{III}\square$-F, Ti^{IV}_2Mg-F, $Ti^{III}Mg\square$-F
4.7	34.5	54.7	$Ti^{IV}_2\square$-F, $Ti^{IV}Mg\square$-F, $Ti^{III}\square_2$-F

5. Proportions of anionic environments in the vicinity of the vacancy, *i.e.*, $\square X_6$ with X = F, O(OH)

Table S2. Estimated proportions of fluorine species (%) from the relative intensities of their ^{19}F NMR lines,[1,3] average F coordination number (F CN) and O(OH) coordination number (O(OH) CN) in $Ti_{1-x-y}\square_{x+y}O_{2-4(x+y)}F_{4x}(OH)_{4y}$ samples.

Sample	Ti_3-F	$Ti_2\square$-F	$Ti\square_2$-F	F CN	O(OH) CN
$Ti_{0.78}\square_{0.22}O_{1.12}F_{0.40}(OH)_{0.48}$	4.4	63.7	31.9	1.73	2.55
$Ti_{0.87}\square_{0.13}O_{1.48}F_{0.36}(OH)_{0.16}$	4.6	64.8	30.6	1.74	2.80

Table S3. Estimated proportions of the anions (F, O(OH), %) in the vicinity of titanium atoms (Ti) and vacancies (□) in $Ti_{1-x-y}\square_{x+y}O_{2-4(x+y)}F_{4x}(OH)_{4y}$ samples.

Sample		Ti	□
$Ti_{0.78}\square_{0.22}O_{1.12}F_{0.40}(OH)_{0.48}$	F	14.7	38.6
	O(OH)	85.3	61.4
$Ti_{0.87}\square_{0.13}O_{1.48}F_{0.36}(OH)_{0.16}$	F	12.0	58.2
	O(OH)	88.0	41.8

Table 4. Estimated proportions of anionic environments in the vicinity of titanium (TiX_6) and vacancy ($\square X_6$) assuming random distributions of the anions (X = F, O(OH)) in $Ti_{1-x-y}\square_{x+y}O_{2-4(x+y)}F_{4x}(OH)_{4y}$ samples.

Sample	$Ti_{0.78}\square_{0.22}O_{1.12}F_{0.40}(OH)_{0.48}$		$Ti_{0.87}\square_{0.13}O_{1.48}F_{0.36}(OH)_{0.16}$	
	TiX_6	$\square X_6$	TiX_6	$\square X_6$
6 O(OH)	38.4%	5.3%	46.4%	0.5%
5 O(OH), 1 F	39.8%	20.2%	38.0%	4.5%
4 O(OH), 2 F	17.2%	31.7%	13.0%	15.6%
3 O(OH), 3 F	4.0%	26.7%	2.4%	28.8%
2 O(OH), 4 F	0.5%	12.6%	0.2%	30.0%
1 O(OH), 5 F	0.0%	3.2%	0.0%	16.7%
6 F	0.0%	0.3%	0.0%	3.9%

6. Density Functional Theory (DFT) calculations

Our density functional theory (DFT) calculations were performed using the VASP,[12,13] with valence electrons described by a plane-wave basis with a cutoff of 500 eV. Interactions between core and valence electrons were described using the projector augmented wave (PAW) method,[14] with cores of [Ar] for Ti, [He] for O, [He] for F, [Ne] for Mg, and [H^+] for H. The calculations used the revised Perdew-Burke-Ernzerhof generalized gradient approximation function PBEsol,[15] with a Dudarev +*U* correction applied to the Ti d states (GGA+*U*).[16–18] We used a value of $U_{Ti,d}$=4.2 eV, which has previously been used to model intercalation of lithium and other metal ions in stoichiometric and defective anatase TiO_2.[4,17–19] To model anatase TiO_2, we first performed a full geometry optimisation on a single Ti_4O_8 unit cell, with optimized lattice parameters obtained by fitting a series of constant volume calculations to the Murnaghan equation of state.[20] All subsequent calculations were fixed to the resulting optimised lattice parameters. Intercalation into stoichiometric anatase TiO_2 was modelled using a 4 × 4 × 2 supercell (384 atoms), with a single Mg ion inserted at an interstitial site ($MgTi_{128}O_{256}$). To identify the preferred positions of F^- and OH^- anions in relation to a cationic Ti vacancy, we performed a series of calculations in 4 × 4 × 2 supercells, with 1 Ti vacancy, and 4 charge compensating X_O species, with *X*=(F, OH), giving cell stoichiometries of $Ti_{127}O_{252}X_4$. These calculations agree with our previous study, that found that fluoride ions preferentially occupy sites adjacent to the titanium vacancy in equatorially-coordinated sites.[1] We find that OH shows the same preference for occupying anion sites adjacent to the titanium vacany.[21] Magensium intercalation into $Ti_{1-x-y}\square_{x+y}O_{2-4(x+y)}F_{4x}(OH)_{4y}$ was modelled using 4 × 4 × 2 supercells, with 1 Ti vacancy, and 4 charge compensating X_O species (*X*=F, OH) occupying four anion sites adjacent to the vacancy. We calculated intercalation energiesfor 4*X*=(4F, 3F+OH, 2F+2OH, F+3OH, and 4OH). In the case of 4*X*=2F+2OH, we considered like anions arranged in an opposite (trans) equatorial site pair configuration. We have previously shown that this gives a similar intercalation energy as for the adjacent (cis) equatorial site pair configuration.[21] Calculations of the intercalation energy of Mg at vacancy-adjacent sites were performed using the same 4 × 4 × 2 cell. For each anion combination considered, we placed a Mg ion at each of eight adjacent interstitial sites and performed a geometry optimization keeping the cell shape and volume fixed.

Individual calculations were deemed optimised when all atomic forces were smaller than 0.01 eV $Å^{-1}$. All calculations were spin polarized, and used a 4 × 4 × 2 Monkhorst-Pack grid for sampling *k*-space in the single unit cell, and only the gamma-point for the 4 × 4 × 2 cells. To calculate intercalation energies, reference calculations for metallic Mg was performed using the same convergence criteria as above. We considered a 2-atom cell for Mg, with a 16 × 16 × 16 Monkhorst-Pack grid for *k*-space sampling. Data sets containing these DFT calculation inputs and outputs are available at the University of Bath Data Archive[20,22]. Code to produce figure 3b from these data is included in dataset Ref 22.

Analysis scripts containing calculations of competing anion configurations are available as part of an open-source repository as reference,[21] published under the MIT license.

References

1 W. Li, D. Corradini, M. Body, C. Legein, M. Salanne, J. Ma, K. W. Chapman, P. J. Chupas, A.-L. Rollet, C. Julien, K. Zhagib, M. Duttine, A. Demourgues, H. Groult and D. Dambournet, *Chem. Mater.*, 2015, **27**, 5014–5019.

2 W. Li, M. Body, C. Legein, O. J. Borkiewicz and D. Dambournet, *Eur. J. Inorg. Chem.*, 2017, **2017**, 192–197.

3 J. Ma, W. Li, B. J. Morgan, J. Światowska, R. Baddour-Hadjean, M. Body, C. Legein, O. J. Borkiewicz, S. Leclerc, H. Groult, F. Lantelme, C. Laberty-Robert and D. Dambournet, *Chem. Mater.*, 2018, **30**, 3078–3089.

4 T. Koketsu, J. Ma, B. J. Morgan, M. Body, C. Legein, W. Dachraoui, M. Giannini, A. Demortière, M. Salanne, F. Dardoize, H. Groult, O. J. Borkiewicz, K. W. Chapman, P. Strasser and D. Dambournet, *Nat. Mater.*, 2017, **16**, 1142.

5 C. J. Wen, B. A. Boukamp, R. A. Huggins and W. Weppner, *J. Electrochem. Soc.*, 1979, **126**, 2258–2266.

6 D. Fattakhova, L. Kavan and P. Krtil, *J. Solid State Electrochem.*, 2001, **5**, 196–204.

7 E. Talaie, P. Bonnick, X. Sun, Q. Pang, X. Liang and L. F. Nazar, *Chem. Mater.*, 2017, **29**, 90–105.

8 Y. Ishii, N. P. Wickramasinghe and S. Chimon, *J. Am. Chem. Soc.*, 2003, **125**, 3438–3439.

9 D. Massiot, F. Fayon, M. Capron, I. King, S. Le Calvé, B. Alonso, J.-O. Durand, B. Bujoli, Z. Gan and G. Hoatson, *Magn. Reson. Chem.*, 2002, **40**, 70–76.

10 A. Sadoc, M. Body, C. Legein, M. Biswal, F. Fayon, X. Rocquefelte and F. Boucher, *Phys. Chem. Chem. Phys.*, 2011, **13**, 18539–18550.

11 J. Ma, W. Li, B. J. Morgan, J. Swiatowska, R. Baddour-Hadjean, M. Body, C. Legein, O. J. Borkiewicz, S. Leclerc, H. Groult, F. Lantelme, C. Laberty-Robert and D. Dambournet, *Chem. Mater.*, 2018, 30, 3078–3089.

12 G. Kresse and J. Hafner, *J. Phys. Condens. Matter*, 1994, **6**, 8245.

13 G. Kresse and J. Furthmüller, *Phys. Rev. B*, 1996, **54**, 11169–11186.

14 G. Kresse and D. Joubert, *Phys. Rev. B*, 1999, **59**, 1758–1775.

15 S. L. Dudarev, A. I. Liechtenstein, M. R. Castell, G. A. D. Briggs and A. P. Sutton, *Phys. Rev. B*, 1997, **56**, 4900–4908.

16 S. L. Dudarev, G. A. Botton, S. Y. Savrasov, C. J. Humphreys and A. P. Sutton, *Phys. Rev. B*, 1998, **57**, 1505–1509.

17 B. J. Morgan and G. W. Watson, *Phys. Rev. B*, 2010, **82**, 144119.

18 B. J. Morgan and G. W. Watson, *J. Phys. Chem. Lett.*, 2011, **2**, 1657–1661.

19 W. Li, M. Fukunishi, B. J. Morgan, O. J. Borkiewicz, V. Pralong, A. Maignan, H. Groult, S. Komaba and D. Dambournet, *Inorg. Chem. Front.*, , DOI:10.1039/C8QI00185E.

20 B. J. Morgan, DFT dataset: *X=(Li,Na,Ca,Mg,Al) Intercalation into (F/OH)-Substituted Anatase TiO_2*, https://researchdata.bath.ac.uk/473/, (accessed April 30, 2018).

21 B. J. Morgan, *DFT Data Analysis: Intercalation of X=(Li, Na, Mg, Ca, Al) into (F/OH)-substituted anatase TiO_2*, Zenodo, 2018.

22 B. J. Morgan, *DFT Dataset: Mg Intercalation into (OH,F)-Substituted Anatase TiO_2*, doi on publication.